

Probabilistic fracture toughness prediction of composite materials

†Yan Li^{1*}, Min Zhou²

¹Department of Mechanical and Aerospace Engineering, California State University, Long Beach, USA.

²The George W. Woodruff School of Mechanical Engineering, School of Materials Science and Engineering
Georgia Institute of Technology, Atlanta, GA 30332-0405, U.S.A.

*Presenting author: yan.li@csulb.edu

†Corresponding author: yan.li@csulb.edu

Abstract

One of the biggest challenges in material sensitive design is to predict the variation of key material properties such as strength and fracture toughness. It has been proved that the stochastic nature of microstructure is the primary reason for fracture toughness scatter. Although Weibull distribution has been widely used to determine the probability of material fracture, its role has been confined to fitting fracture toughness data rather than providing predictive insight of material fracture toughness and the magnitude of scatter. Besides, the Weibull parameters which are obtained through curve fitting carry little physical significance. In this paper, an integrated computational and analytical model is developed to predict fracture toughness in a statistical sense. The Weibull distribution parameters are correlated with the statistical measures of microstructure characteristics and the statistical characterization of the competition between crack deflection and crack penetration at matrix/reinforcement interfaces. The approach and model will lead to more reliable material design through microstructure tailoring.

Keywords: Microstructure, Fracture toughness, Weibull distribution

Introduction

Fracture toughness of a composite material is not a deterministic property. This is primarily due to the stochastic nature the crack-microstructure interactions [1-3]. Most of the existing probabilistic models for fracture toughness prediction only consider near crack-tip stress states [4-6]. Information regarding microstructure of its microstructure as well as the activation of different fracture mechanisms during characteristics and failure mechanisms associated with the crack propagation process is not explicitly included in the model formulations. He and Hutchinson [7] used the energy criterion to analyze the behavior of a semi-infinite crack perpendicular to an infinite planar interface in a symmetrically loaded, isotropic bi-material. They concluded that crack deflection occurs when

$$J_d / J_p > \Phi_{in} / \Phi_p. \quad (1)$$

Here, J_d and J_p denote the energy release rate for crack deflection and crack penetration, respectively. Similarly, Φ_{in} and Φ_p denote the surface energy of the interface and reinforcement, respectively.

Gupta et al. [8] extended He and Hutchinson's work to anisotropic materials and developed a strength criterion for crack deflection and validated their analysis using laser spallation experiments. Subsequently, Martinez and Gupta [9] improved the criterion such that it does not require any assumption concerning crack extension ratio by using a quasi-static approximation and by assuming that deflection occurs under constant loading. Although these models reveal some of the fundamental relations that govern the behavior of cracks as they approach interfaces, the analyses concern the interaction between a single crack and an infinite, flat interface. These criteria cannot be directly applied to real composite materials analysis due to the following reasons. First of all, the reinforcements in real composite materials have finite size. Therefore, the interface cannot be considered as infinite. Besides, it has been proved that the shape of reinforcements also influence the activation of different fracture mechanisms. The shape of reinforcements needs to be quantified and included in the criterion as well.

Based on the previous work, Li and Zhou [10] further extend He and Hutchinson's criterion by including the effects of finite reinforcement size, reinforcement shape and distribution in a two-phase composite material. The criterion is parameterized by

$$U = \frac{1 - \beta^2}{a_0(1 - \alpha)} \left[|c|^2 + |h|^2 + 2R_e(ch) \right] \bar{\rho}^{a_1} e^{\left(\frac{a_2}{s}\right)} - \frac{\Phi_{in}}{\Phi_p}, \quad (2)$$

to determine the activation of the two competing failure mechanisms. Specifically, interface debonding, which is activated by crack deflection, is predicted when $U > 0$. Otherwise, crack penetration induced reinforcement cracking will be activated instead. In the above relation, $\bar{\rho}$ is the roundness of the reinforcement. s represents the characteristic reinforcement size. Φ_{in} and Φ_p are the surface energies of the interface and reinforcement, respectively.

Based on the previous work, an integrated computational and analytical model is introduced which allows the possible range of fracture toughness values to be predicted as function of microstructure. The Weibull distribution parameters are directly correlated to the two-point correlation functions as well as the quantification of fracture mechanisms. These relations can be used for material reliability design by controlling the fracture toughness scatter through microstructure tailoring.

Cohesive Finite Element Method (CFEM) based fracture toughness prediction

The edge-cracked square specimen under Mode I tensile loading in Fig. 1 has a size length of 3.65 mm. The microstructure region has a length of 2 mm, width of 1 mm and a pre-crack length of 0.73 mm. A boundary velocity of $v = 5$ mm/s is imposed at the top and bottom edges. The remaining edges of the specimen are traction-free. Conditions of plane strain are assumed to prevail. In the following analysis, we consider TiB_2 reinforced Al_2O_3 composites.

Cohesive elements are embedded along the edge of each bulk element in the microstructure region. Bilinear traction separation law is employed. This law is derived from a potential Φ which is a function of separation vector Δ through a state variable defined as

$\lambda = \sqrt{(\Delta_n/\Delta_{nc})^2 + (\Delta_t/\Delta_{tc})^2}$. This variable describes the effective instantaneous state of mixed-mode separations. Here, $\Delta_n = \mathbf{n} \cdot \Delta$ and $\Delta_t = \mathbf{t} \cdot \Delta$ denote, respectively, the normal and tangential components of Δ , with \mathbf{n} and \mathbf{t} being unit normal and tangent vectors. Δ_{nc} is the critical normal separation at which the cohesive strength of an interface vanishes under conditions of pure normal deformation ($\Delta_t = 0$). Similarly, Δ_{tc} is the critical tangential separation at which the cohesive strength of an interface vanishes under conditions of pure shear deformation ($\Delta_n = 0$). λ tracks instantaneous mixed-mode separations during both loading and unloading. Apparently, $\lambda = 0$ corresponds to $\Delta = 0$ (undeformed state or fully unloaded state) and $\lambda \geq 1$ implies complete separation, i.e. total debonding of the cohesive surface pair.

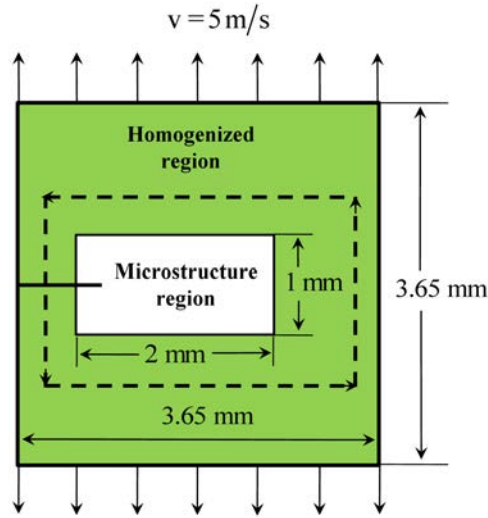


Fig. 1 Specimen configuration used in the analysis.

CFEM models with traction-separation laws with finite initial stiffness have two competing requirements on element size. The upper bound requires that the element size must be small enough to accurately resolve the stress distribution inside the cohesive zones at crack tips. The lower bound, on the other side, requires the cohesive surface induced stiffness reduction be small, such that the wave speed in the solid is not significantly affected due to the presence of the cohesive surfaces. For the conditions of this paper, the preferred range of the element size is $7 \mu\text{m} \ll h \ll 14 \mu\text{m}$, allowing the convergence criterion in Tomar et al. [11] to be satisfied.

For brittle materials, the fracture toughness K_{IC} is related to the energy release rate J_{IC} as

$$K_{IC} = \sqrt{J_{IC} \frac{\bar{E}}{1-\bar{\nu}^2}}, \quad (3)$$

where \bar{E} and $\bar{\nu}$ are the effective Young's modulus and effective Poisson's ratio of the heterogeneous material, respectively. \bar{E} and $\bar{\nu}$ are estimated by using the Mori-Tanaka method as

$$\begin{cases} \bar{E} = \frac{9\bar{K}\bar{\mu}}{3\bar{K} + \bar{\mu}} \text{ and} \\ \bar{\nu} = \frac{3\bar{K} - 2\bar{\mu}}{6\bar{K} + 2\bar{\mu}}, \end{cases} \quad (4)$$

where \bar{K} and $\bar{\mu}$ are effective bulk and shear moduli. \bar{K} and $\bar{\mu}$ are calculated according to

$$\begin{cases} \bar{K} = K_0 + \frac{f(K_1 - K_0)(3K_0 + 4\mu_0)}{3K_1 + 4\mu_0} \text{ and} \\ \bar{\mu} = \mu_0 + \frac{5f\mu_0(\mu_1 - \mu_0)(3K_0 + 4\mu_0)}{3K_0(3\mu_0 + 2\mu_1) + 4\mu_0(2\mu_0 + 3\mu_1)}. \end{cases} \quad (5)$$

Here, K_r and μ_r represent the bulk and shear modulus, respectively for Al_2O_3 ($r = 0$) and TiB_2 ($r = 1$).

To account for inertia effects, a fully dynamic deformation formulation is used. Within this framework, the path-independent J -integral is (Moran & Shih [12])

$$J = \int_{\Gamma} \left[\left(\int_0^t \boldsymbol{\sigma} : d\boldsymbol{\varepsilon} + \frac{1}{2} \rho \dot{\mathbf{u}} \cdot \dot{\mathbf{u}} \right) dx_2 - \mathbf{t} \cdot \frac{\partial \mathbf{u}}{\partial x_1} ds \right] + \int_A \left(\rho \ddot{\mathbf{u}} \cdot \frac{\partial \mathbf{u}}{\partial x_1} - \rho \dot{\mathbf{u}} \cdot \frac{\partial \dot{\mathbf{u}}}{\partial x_1} \right) dA, \quad (6)$$

where \mathbf{t} is the traction on a surface with normal \mathbf{N} , \mathbf{u} is the displacement, $\boldsymbol{\varepsilon}$ denotes the strain and ρ is the mass density.

The J value in eqn. (6) is integrated along an arbitrary closed contour as shown in the dashed line in Fig. 1. Six snap shots of the crack propagation process in a microstructure with circular TiB_2 reinforcement at a loading velocity of $v = 5$ mm/s is illustrated in Fig. 2(a). The corresponding histories of J and K are shown in Fig. 2(b). Fracture initiates in the Al_2O_3 matrix at $105.0 \mu\text{s}$, this event defines the initiation toughness K_{IC}^i . The crack is arrested by a TiB_2 particle and pauses at the $\text{Al}_2\text{O}_3/\text{TiB}_2$ interface for approximately $42.5 \mu\text{s}$. During the pause, J increases rapidly. At approximately $149.2 \mu\text{s}$, as a result of the higher level of driving force J , the crack penetrates the TiB_2 particle. Subsequently, the crack propagates rapidly, causing J (and therefore K) in Fig. 2 (b) to plateau for the remainder of the analysis. The average value of K during this period is taken as the propagation toughness K_{IC} .

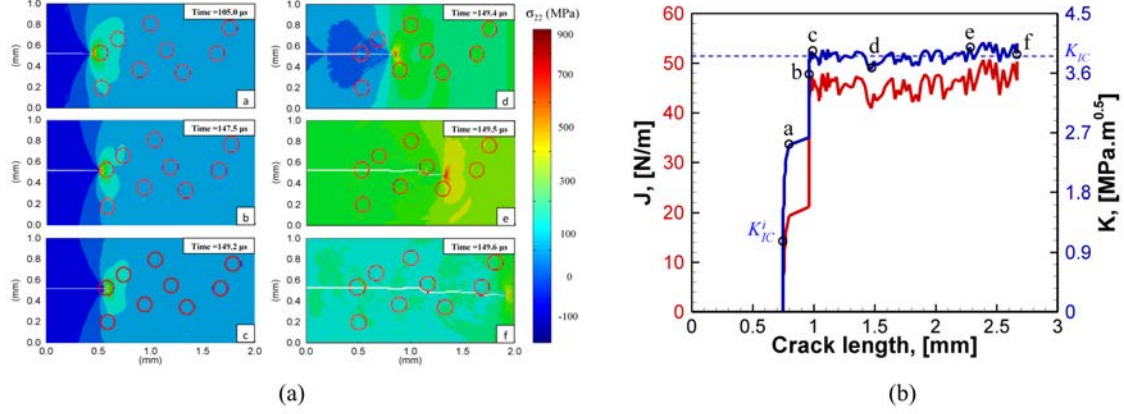


Fig. 2 History of (a) crack propagation in $\text{Al}_2\text{O}_3/\text{TiB}_2$ and the evolution of corresponding J and K .

From the energy point of view, a crack would grow when the energy available in the elastic stress field reaches the energy required to form new fracture surfaces. For crack propagation in a composite material as shown in Fig. 3, new crack surfaces can be created in the matrix, along the interface and in the enforcement. Therefore, J_{IC} can be stated as

$$\begin{aligned}
 J_{IC} &= \frac{\partial U_f}{\partial A} \approx \frac{(\Phi_{in} L_{in} + \Phi_m L_m + \Phi_p L_p) t}{Wt} \\
 &= \frac{L}{W} \left(\Phi_{in} \frac{L_{in}}{L} + \Phi_m \frac{L_m}{L} + \Phi_p \frac{L_p}{L} \right) \\
 &= \xi(R, f) (\Phi_{in} H_{in} + \Phi_m H_m + \Phi_p H_p),
 \end{aligned} \tag{7}$$

where U_f is the total energy released. $A = Wt$ is the total projected crack surface area with W and t being the crack projection length and specimen thickness, respectively. $\xi = L/W$ is a function which captures the tortuosity of the entire crack path. Based on the microstructure configuration discussed before, ξ depends on the R and f . The detailed calculation of H_{in} , H_m and H_p are discussed in detail in Li and Zhou [13].

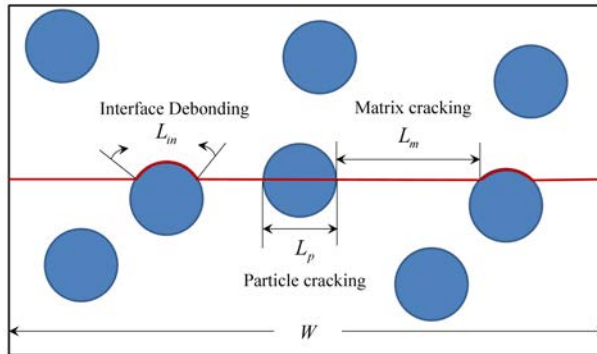


Fig. 3 Schematic illustration of crack lengths associated with different mechanisms in two-phase composite materials.

Probabilistic fracture toughness analysis

A typical two-parameter Weibull distribution function is in the form of

$$P_f = 1 - \exp \left[- \left(\frac{K}{K_0} \right)^m \right]. \quad (8)$$

Here P_f is the probability of fracture. K and K_0 are the fracture toughness K_{IC} measured from experiments and the normalization factor, respectively. m is defined as the shape parameter. The parameters m and K_0 are obtained through a linear regression fit to N data points of K . In order to have a good statistical representation of the stochastic fracture process, $N \geq 20$ is preferred.

In most of the existing probabilistic models, the fracture toughness data is obtained first and then then fitted by Weibull distribution function [14-16]. The problem of these probabilistic models is that they do not allow the scatter of fracture toughness data to be predicted prior to the experimental testing. Without the material sensitivity information, it is hard to determine the number of tests required to obtain a good estimate of probability of material fracture.

Although Weibull parameters in Eqn. (8) are fitting parameters which carry little physical significance, their correlations with microstructure characteristics and fracture mechanisms can provide valuable insight to material sensitive design without doing repeated experimental testing.

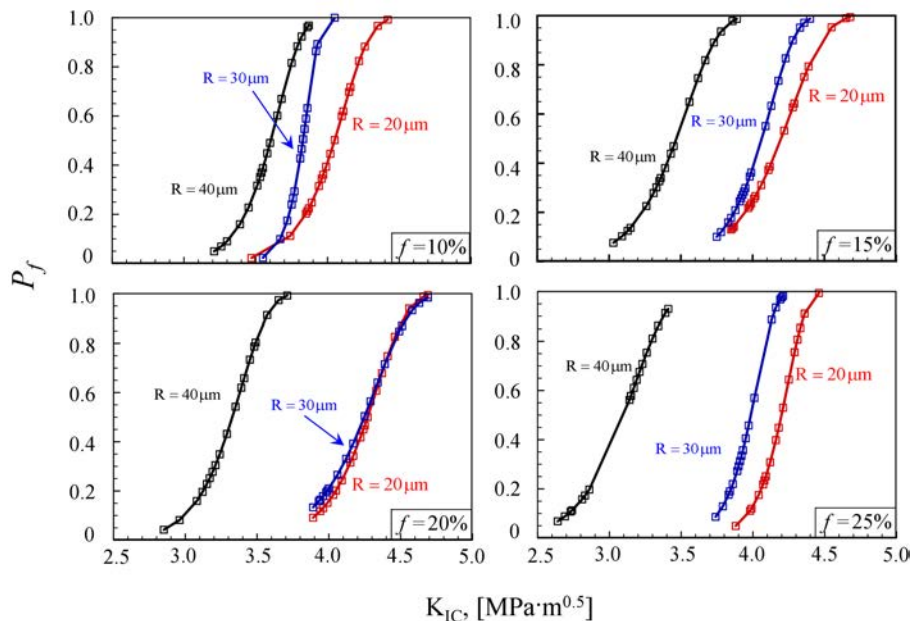


Fig. 4 Fracture probability distribution predicted from CFEM simulations [2] for microstructures with randomly distributed non-overlapping circular particles.

In the following discussions, the K values in Eqn. (8) are calculated from Eqn.(3), Eqn. (6) and Eqn. (7). Microstructures with non-overlapping circular reinforcements are considered. Fig. 4 compares the probability of fracture P_f for microstructures with systematically varying particle radius ($R = 20 \mu\text{m}$, $30 \mu\text{m}$ and $40 \mu\text{m}$) and volume fraction ($f = 10\%$, 15% , 20% and 25%). It is observed that microstructures with smaller radius tend to have higher fracture toughness and lower probability of fracture for all the volume fractions considered. The same trend is observed from the CFEM (Cohesive Finite Element Method) calculations [10] in Fig. 4, where 20 microstructures with same combination of R and f are considered in the analysis. As show in Fig. 5, when f is kept as a constant, the slope of fracture probability curve becomes steeper as R increases, leading to less fracture toughness scatter. The opposite trend is observed when R is fixed while f is increased from 10% to 25%. This indicates that microstructures with fine particles and high volume fractions will have higher-order uncertainties due to the large fracture toughness variation. However, it should be noted that this type of combination also yield higher level fracture toughness values at the same time. This trend has been reported in a few research studies [17-19]. From the microstructure design perspective, it is not surprising that shifting up the fracture toughness values will lead to larger scatter band. First of all, composites materials are toughened through crack-particle interactions. Generally speaking, more interactions during the crack propagation process will lead to higher fracture resistance. If a crack does not encounter any reinforcement, the choice of crack path is very limited. The fracture toughness of the composite material is very close to the fracture toughness of matrix material which is considered as the lower bound fracture toughness. Besides, more crack-particle interactions can be created by increasing the volume fraction of particles. As discussed previously, the effective toughening mechanism during crack-particle interaction is crack deflection induced interface debonding. This requires fine particles in addition to high volume fraction. Crack deflection, which contributes to enhancing the level of fracture toughness, also provides the crack with more opportunities in choosing the path. The scatter is intensified when more crack-particle interactions are included. This explains why microstructure configurations which lead to higher level of fracture toughness also have larger fracture toughness scatter.

It is also noted that the fracture toughness values predicted from Eqn. (3) and (7) is larger than the values predicted from CFEM results. In Fig. 5, the range of K_{IC} values predicted from the analytical model is approximately from $2.7 \text{ MPa}\sqrt{\text{m}}$ to $8.4 \text{ MPa}\sqrt{\text{m}}$. In contrast, the range of K_{IC} values predicted from CFEM calculations only spans from $2.7 \text{ MPa}\sqrt{\text{m}}$ to $4.7 \text{ MPa}\sqrt{\text{m}}$ as shown in Fig. 4. With lower bound K_{IC} predictions being consistent, the analytical model predicts a much higher upper bound value. This is because the two-point correlation functions employed in the analytical model quantify the possibility of crack-particle interactions in the entire microstructure region. However, the crack propagation in CFEM simulations is primarily localized in a small region near the pre-crack plane. The crack does not have the opportunity to interact with particles which are far away from the pre-crack plane. To quantitatively understand how localization of crack propagation influences the level

of fracture toughness and the magnitude of scatter, another set of calculations are carried out by considering the interactions of particles within the local region of each microstructure instantiation employed in CFEM calculations .

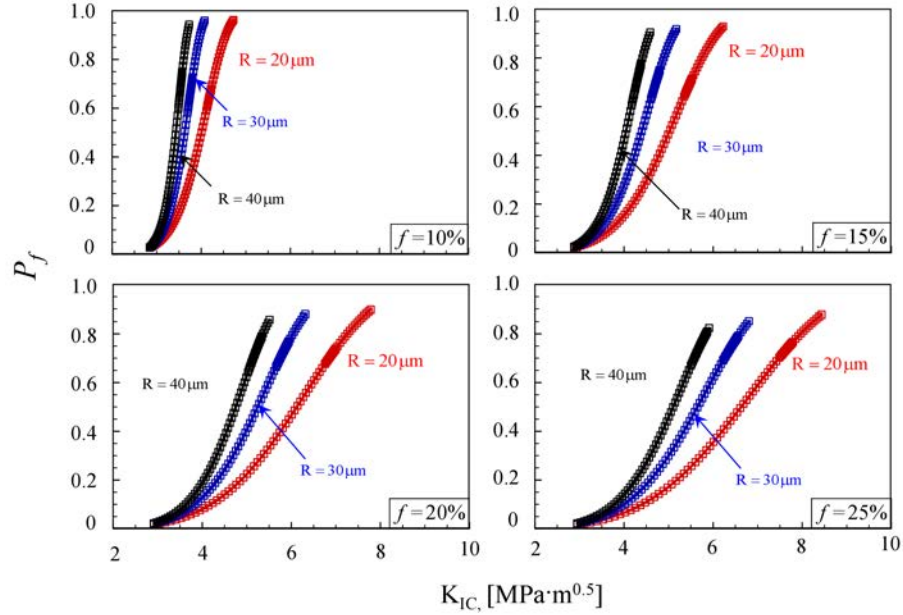


Fig. 5 Fracture probability distribution predicted from analytical model for microstructures with randomly distributed non-overlapping circular particles.

Fracture toughness scatter is quantified by the shape parameter m . It can be inferred from Eqn. (8) that if the magnitude of the scatter is large, then m is small and vice versa. Specially, $m \rightarrow \infty$ is expected if there is no scatter. Theoretically, it can be achieved only when $f = 0$ or $f = 1$ as the microstructure is purely matrix phase or reinforcement phase.

Fig. 6 compares m values predicted from the analytical model and CFEM framework. The solid lines and dashed lines represent analytical solutions with the entire microstructure and local microstructure region, respectively. CFEM results are illustrated by dots. Microstructures considered here have volume fraction f ranging from 0 to 30%. Three particle sizes with $R = 20 \mu\text{m}$, $R = 30 \mu\text{m}$ and $R = 40 \mu\text{m}$ are employed and represented by blue, red and black color, respectively. As demonstrated in Fig. 6, a much higher level of m values are predicted for analytical solutions considering the local microstructure region. This means there is smaller fracture toughness scatter when the crack only propagates in the localized microstructure region. It makes sense that a lower level of m values are predicted when the entire microstructure region is considered since the interactions of crack with all the particles in the microstructure region are included. From microstructure design prospective, m values predicted by considering the entire microstructure region are very conservative since the crack-particle interaction is usually localized when the reinforcements are well bonded with the matrix. Therefore, analysis with local and entire microstructure region can serve as the upper limit and lower limit of m as represented by dashed and solid lines, respectively. Despite discrepancies in m , both predictions share the same trends. First of all, the increase

of volume fraction f leads to decreased m . The larger scatter of fracture toughness is observed due to more intensified crack-particle interactions during crack propagation. The decrease of R can have the same effect as small particles promote interface debonding and create more uncertainties in choosing the crack path. It is noted that the CFEM predictions of m all fall between the upper and lower bound with the similar trends as observed from the analytical predictions. It is also observed that the CFEM predictions are closer to the upper bound m as f increases. When $f = 25%$, m values predicted from CFEM calculations are very close to the upper bound prediction especially when particle size is small. It can be inferred that the crack-particle interactions in local microstructure region is representative of the entire microstructure region when reinforcements with small size and large volume fractions are considered. As shown in Fig. 6, the discrepancy between the lower bound curves and upper bound curves becomes smaller with increasing f and decreasing R . Once f increases to 100% and R decreases to 0, both the upper and lower bound curves will saturate to $m \rightarrow \infty$ as the microstructure becomes pure reinforcement phase. This means m will not continue to decrease as f increases. After f reaches a critical value, the trend reverses. Although the critical f cannot be predicted because the analytical model developed here only considers non-overlapping circular reinforcements, the trends observed from the above analysis are still valid for most engineering cases.

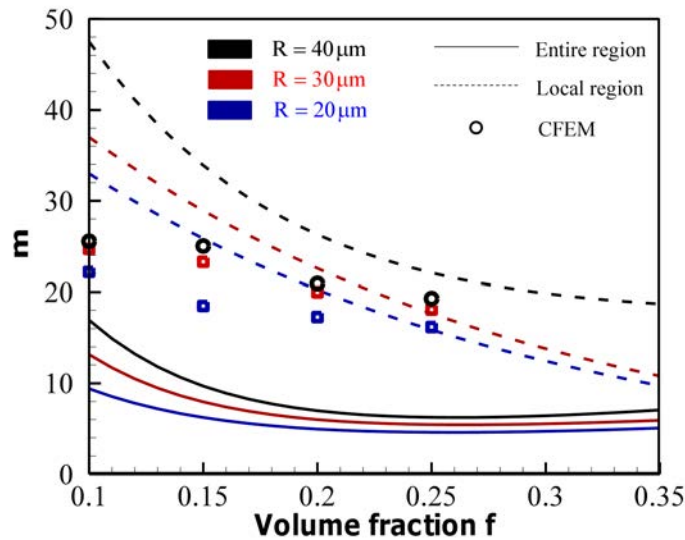


Fig. 6 Effect of microstructure attributes on m predicted from CFEM model and analytical model considering the entire and local microstructure region, respectively.

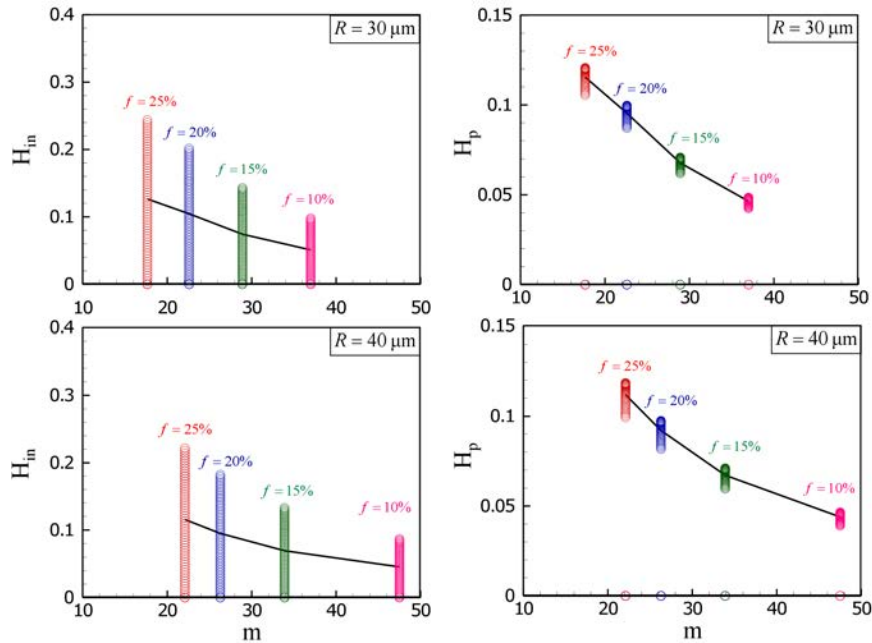


Fig. 7 Effect of proportions of interface debonding H_{in} and particle cracking H_p on m under different values of particle size and volume fraction.

Fig. 7 summarizes the scatter of H_{in} and H_p under different particle size and volume fraction, and compares them with the scatter of fracture toughness m . H_{in} , H_p and m are all predicted from the analytical model considering the local microstructure region. The solid black line in each sub-figure connects the average value of H_{in} or H_p under each volume fraction. It is noted that the scatter of fracture toughness primarily comes of the scatter of H_{in} . The increase in volume fraction f and decrease in particle size R can lead to higher average H_{in} and higher H_{in} as well. Compared with H_{in} , H_p is less sensitive to R and f . The increase in volume fraction f and particle size R has limited effect on the average value of H_p and its scattering.

Conclusions

In conclusion, the most effective way to improve the fracture toughness of two-phase composite material is to increase crack tortuosity by promoting interface debonding. This can be achieved by introducing refined second-phase reinforcements with adequate volume fraction. It should be noted that the decrease in reinforcement size and increase in volume fraction also enhance the sensitivity of the material system as larger fracture toughness scatter is observed at the same time. The analytical model developed here provide a way to estimate the upper and lower limit of fracture toughness by considering microstructure attributes and fracture mechanisms involved in the failure process. The prediction of Weibull parameter m

as shown in Fig. 6 can be employed as a reference of fracture toughness scatter for material sensitive design of two-phase composite materials.

References

- [1] K. Strecker, S. Ribeiro, R. Oberacker, and M. J. Hoffmann, "Influence of microstructural variation on fracture toughness of LPS-SiC ceramics," *International Journal of Refractory Metals & Hard Materials*, vol. 22, pp. 169-175, 2004.
- [2] Y. Li and M. Zhou, "Prediction of fracture toughness of ceramic composites as function of microstructure: I. Numerical simulations," *Journal of the Mechanics and Physics of Solids*, vol. 61, pp. 472-488, Feb 2013.
- [3] S. Lee, T. H. Kim, and D. Kwon, "Microstructural Analysis of Fracture-Toughness Variation in 2xxx-Series Aluminum-Alloy Composites Reinforced with Sic Whiskers," *Metallurgical and Materials Transactions a-Physical Metallurgy and Materials Science*, vol. 25, pp. 2213-2223, Oct 1994.
- [4] T. L. Becker, R. M. Cannon, and R. O. Ritchie, "Statistical fracture modeling: crack path and fracture criteria with application to homogeneous and functionally graded materials," *Engineering Fracture Mechanics*, vol. 69, pp. 1521-1555, Sep 2002.
- [5] B. Z. Margolin, A. G. Gulenko, and V. A. Shvetsova, "Probabilistic model for fracture toughness prediction based on the new local fracture criteria," *International Journal of Pressure Vessels and Piping*, vol. 75, pp. 307-320, Apr 1998.
- [6] A. Valiente, J. Ruiz, and M. Elices, "A probabilistic model for the pearlite-induced cleavage of a plain carbon structural steel," *Engineering Fracture Mechanics*, vol. 72, pp. 709-728, Mar 2005.
- [7] H. Ming-Yuan and J. W. Hutchinson, "Crack deflection at an interface between dissimilar elastic materials," *International Journal of Solids and Structures*, vol. 25, pp. 1053-1067, // 1989.
- [8] V. Gupta, J. Yuan, and D. Martinez, "Calculation, Measurement, and Control of Interface Strength in Composites," *Journal of the American Ceramic Society*, vol. 76, pp. 305-315, 1993.
- [9] D. Martínez and V. Gupta, "Energy criterion for crack deflection at an interface between two orthotropic media," *Journal of the Mechanics and Physics of Solids*, vol. 42, pp. 1247-1271, 1994/08/01 1994.
- [10] Y. Li and M. Zhou, "Prediction of fracture toughness of ceramic composites as function of microstructure: II. analytical model," *Journal of the Mechanics and Physics of Solids*, vol. 61, pp. 489-503, 2// 2013.
- [11] V. Tomar, J. Zhai, and M. Zhou, "Bounds for element size in a variable stiffness cohesive finite element model," *International Journal for Numerical Methods in Engineering*, vol. 61, pp. 1894-1920, Nov 21 2004.
- [12] B. Moran and C. F. Shih, "A general treatment of crack tip contour integrals," *International Journal of Fracture*, vol. 35, pp. 295-310, 1987.
- [13] Y. Li and M. Zhou, "Prediction of fracture toughness scatter of composite materials," *Computational Materials Science*, vol. 116, pp. 44-51, Apr 15 2016.
- [14] W. Weibull, "A statistical theory of the strength of materials," *Ing. Vetenskaps Akad. Handl.151.*, pp. 1-45, 1939.
- [15] K. Wallin, "Macroscopic Nature of Brittle-Fracture," *Journal De Physique Iv*, vol. 3, pp. 575-584, Nov 1993.
- [16] K. Wallin, K. Torronen, R. Ahlstrand, B. Timofeev, V. Rybin, V. Nikolaev, *et al.*, "Theory Based Statistical Interpretation of Brittle-Fracture Toughness of Reactor

- Pressure-Vessel Steel 15x2m-Phi-a and Its Welds," *Nuclear Engineering and Design*, vol. 135, pp. 239-246, Jun 1992.
- [17] K. V. Logan, "Composite Ceramics, Final Tehnical Report, final technical report," ed: USSTACOM DAAEO7-95-C-R040, 1996.
- [18] A. G. Evans, "Perspective on the Development of High-Toughness Ceramics," *Journal of the American Ceramic Society*, vol. 73, pp. 187-206, Feb 1990.
- [19] T. Lin, A. G. Evans, and R. O. Ritchie, "Statistical-Analysis of Cleavage Fracture Ahead of Sharp Cracks and Rounded Notches," *Acta Metallurgica*, vol. 34, pp. 2205-2216, Nov 1986.